Molecular Crystals and Liquid Crystals

ISSN: 1542-1406 (Print) 1563-5287 (Online) Journal homepage: http://www.tandfonline.com/loi/gmcl20

# Effect of the Sintering Temperature on the Structure and Properties of Fe-doped $Bi_{3.25}La_{0.75}Ti_2O_{12}$ Ceramics

Do Hyun Kim, Jun Young Han & Chung Wung Bark

**To cite this article:** Do Hyun Kim, Jun Young Han & Chung Wung Bark (2015) Effect of the Sintering Temperature on the Structure and Properties of Fe-doped $Bi_{3.25}La_{0.75}Ti_2O_{12}$ Ceramics, Molecular Crystals and Liquid Crystals, 621:1, 129-135, DOI: 10.1080/15421406.2015.1096447

**To link to this article:** http://dx.doi.org/10.1080/15421406.2015.1096447

*Mol. Cryst. Liq. Cryst.*, Vol. 621: pp. 129–135, 2015

ISSN: 1542-1406 print/1563-5287 online
DOI: 10.1080/15421406.2015.1096447



# Effect of the Sintering Temperature on the Structure and Properties of Fe-doped $Bi_{3.25}La_{0.75}Ti_2O_{12}$ Ceramics

DO HYUN KIM, JUN YOUNG HAN, AND CHUNG WUNG BARK*

Department of Electrical Engineering, Gachon University, Seongnam, Gyeonggi, Republic of Korea

*Recently, ferroelectric materials, such as La-substituted bismuth titanate ($Bi_{3.25}La_{0.75}Ti_3O_{12}$, BLT), have attracted interest for their potential applications in nano-electronics and nano-optoelectronics. On the other hand, the wide band gap of BLT has limited its opto-electronics applications. To solve this wide band gap problem in complex oxides, Fe doped BLT ($Bi_{3.25}La_{0.75}FeTi_2O_{12}$, Fe-BLT) could result in a dramatic decrease in the band gap without breaking its crystallographic symmetry. To fabricate the opto-electric devices, a bulk ceramic target was synthesized using Fe-BLT for thin film growth. To determine the optimal temperature, the pellets were sintered at different temperatures ranging from 700°C–1100°C for 2.5 hours. This study found that Fe-BLT target can be sintered at 1000°C without an impurity phase with comparable density and hardness to a target sintered at higher temperatures.*

**Keywords** Sintering Temperature; Target; Thin film

## Introduction

Ferroelectric thin films have many applications, such as high dielectric constant capacitors, dynamic random access memories with a low switching voltage, electro-optic devices, uncooled infrared detectors, and focal plane arrays [1–2]. This is because ferroelectric thin films with large remanent polarization, low coercive field and low fatigue rate characteristics have potential use as memory elements in high density 1T-1C nonvolatile memory [3].

In many ferroelectric materials, bismuth titanate ($Bi_4Ti_3O_{12}$, BIT) thin films have attracted considerable attention because of the excellent electro-optic and ferroelectric properties arising from its uniform Bi-layered perovskite structure [4]. On the other hand, the disadvantages of low remnant polarization ($P_r$) and high coercive field ($E_c$) have limited the applications of BIT in the field of electronic devices.

To improve the ferroelectric properties of materials, many studies have attempted to substitute ions in BIT. In the case of A-site substitution in BIT, Park et al. studied lanthanides, such as La-, Pr-, Sm-, and Nd-substituted BIT films, and reported that La-substituted BIT

*Address correspondence to Chung Wung Bark, Department of Electrical Engineering, Gachon University, Seongnam, Gyeonggi 461-701, Republic of Korea. E-mail: bark@gachon.ac.kr

Color versions of one or more of the figures in the article can be found online at www.tandfonline.com/gmcl.

($Bi_{3.25}La_{0.75}Ti_3O_{12}$, BLT) films have a large $P_r$, low processing temperature and fatigue-free characteristics [5].

Recently, W.S. Choi et al. reported that layered ferroelectric BLT by site-specific substitution can reduce the band gap while remaining strongly ferroelectric. The technique to tune the band gap is becoming increasingly important for the development of highly efficient solar cells and transparent conducting oxides [6]. For example, lower band gap ferroelectrics oxides, such as $BiFeO_3$ (BFO) of only 2.7 eV [7] have applications in photovoltaic or photocatalytic devices. The photovoltaic effects in BFO have the highest efficiency because of the large saturation polarization (∼90 $C/cm^2$) and lower band gap ($E_g$∼2.67 eV) than many other ferroelectric perovskites [8–9]. Gao, F.*et al*. reported that BFO nanoparticles exhibit photocatalytic activity under visible light irradiation because of the small bandgap [10].

On the other hand, BLT films have a considerable influence on the ferroelectric and optical properties but the impact on the band structure is quite small. As a result, BLT has a wide band gap of more than 3.0 eV [11]. To solve the wide band gap problem in complex oxides, cobalt or iron doping on BLT were synthesized using a simple chemical reaction method. The results showed that the Fe doped BLT ($Bi_{3.25}La_{0.75}FeTi_2O_{12,}$ Fe-BLT) could decrease the band gap dramatically without breaking their crystallographic symmetry [12–13].

To apply the bulk target material to electro-devices, it is important to deposit thin film. Normally, the density of bulk ceramic targets and the degree of uniformity of their microstructure have a significant impact on the quality of thin film. Therefore, an effective way of increasing the density of a bulk ceramic target for thin film growth is presented. One of best methods is the increase in sintering temperature during the synthesis of a bulk ceramic target. In the case of undoped and Mn-doped BLT, $WO_3$-doped BLT sintered at 1100°C, X-ray diffraction (XRD) revealed an orthorhombic structure without a second phase [14–16].

On the other hand, in the case of Fe doping, because of the high reactivity of iron, the XRD data of the Fe-BLT bulk ceramic target sintered at 1100°C showed a significant amount of impurity phase and a change in crystallinity.

Fe-BLT ceramic targets that were fabricated at different sintering temperatures (700∼1100°C) were studied to determine the optimal sintering temperature for the Fe-BLT bulk ceramic target. The sintering temperature needs to be optimized to obtain the proper densification of the pellets without abnormal grain growth. In the case of fine powders, the necessary diffusion length of the atoms for the purpose of sintering becomes shorter. This accelerates pore diffusion, giving rise to high density ceramics. The structural properties of the pelletized samples were examined by XRD and SEM. As a result, the Fe-BLT target sintered at 1000°C showed an orthorhombic structure without a second phase and its density was much higher than the samples sintered at other temperatures. Using the Fe-BLT targets sintered at 1000°C, clean Fe-BLT films could be deposited on glass substrates by 90°off–axis RF sputtering.

### *Experimental Procedure*

The samples were synthesized by a solid-state reaction using the following starting binary oxide powders: $Bi_2O_3$ (99.9%, Kojundo), $TiO_2$ (99.99%, Kojundo), $La_2O_3$ (99.99%, Kojundo), and $Fe_2O_3$ (99.9%, Kojundo). The powders were blended thoroughly at the stoichiometric ratio in a ball mill for 24 hours, dried in an oven at 100°C and calcined at 700°C. The powders were pressed and then sintered at different temperatures ranging from

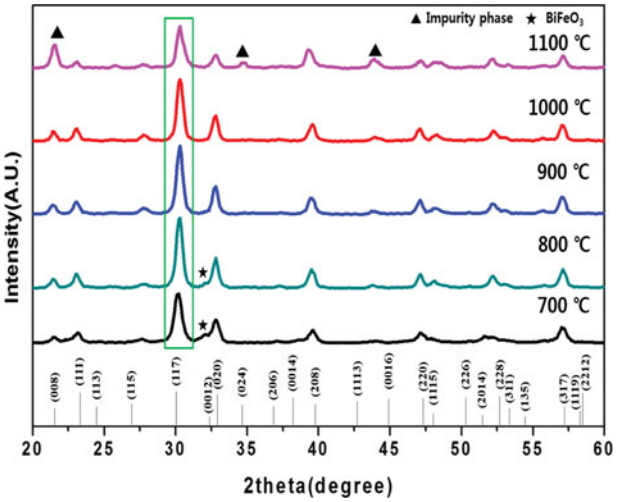


**Figure 1.** XRD patterns of the Fe-BLT pellet sintered at 700, 800, 900, 1000, and 1100°C. The vertical lines indicate the position of ICSD No. 150091.

700°C - 1100°C for 2.5 hours. The pellets were polished and etched thermally to examine their microstructure and morphology. The samples were characterized structurally by XRD (Rigaku, D/MAX 2200) using Cu K$\alpha$ radiation from 20 to 60° 2$\theta$ with an angular step of 0.02°/min. The microstructure of the pelletized powers was examined by SEM (Hitachi, S-4700). The Vickers hardness was measured using a Micro hardness tester (HMV-2) an applied load of 0.98N at room temperature.

### *Results and Discussion*

Figure 1 shows XRD patterns of the Fe-BLT pellet sintered between 700 to 1100°C. The XRD patterns of the pellets sintered at 700°C to 1000°C matched those reported for BLT with an orthorhombic structure (ICSD No. 150091) [15–16]. On the other hand, when the sintering temperature was increased to 1100°C, some other weak XRD peaks were observed, which were not found in the XRD patterns of the materials sintered at other low temperatures, indicating the existence of some impurity phases. The BFO phase was strongly observed at 700°C and 800°C, as confirmed by the JCPDS card no. 71-2494 [17]. The XRD peak intensity of BFO began to decrease from 700 to 900°C because BFO undergoes a phase transition from a ferroelectric $\alpha$-BFO phase to a paraelectric $\beta$-BFO phase from 820 to 830°C [18–19]. Pure Fe-BLT phase formation without a BFO secondary phase was observed at 900 to 1000°C. In addition, the full-width at half maximum (FWHM) of the Fe-BLT main peak (117) decreased from 0.64° to 0.51° when the temperature was increased from 700°C to 1000°C. These suggest that the growth of crystallinity is strongly affected by the sintering temperature.

The morphological and microstructural properties of the samples were examined by SEM. Fig. 2 shows SEM images of the Fe-BLT pellet sintered at (a) 700°C, (b) 800°C, (c) 900°C, (d) 1000°C, and (e) 1100°C. The samples sintered at various temperatures showed a plate-like morphology with a gradually increasing grain size with increasing sintering temperature. Plate-like grain organization was reported to be a typical property of bismuth layer-structured ferroelectrics. Complex oxide materials, such as PZT, BZT, YBCO

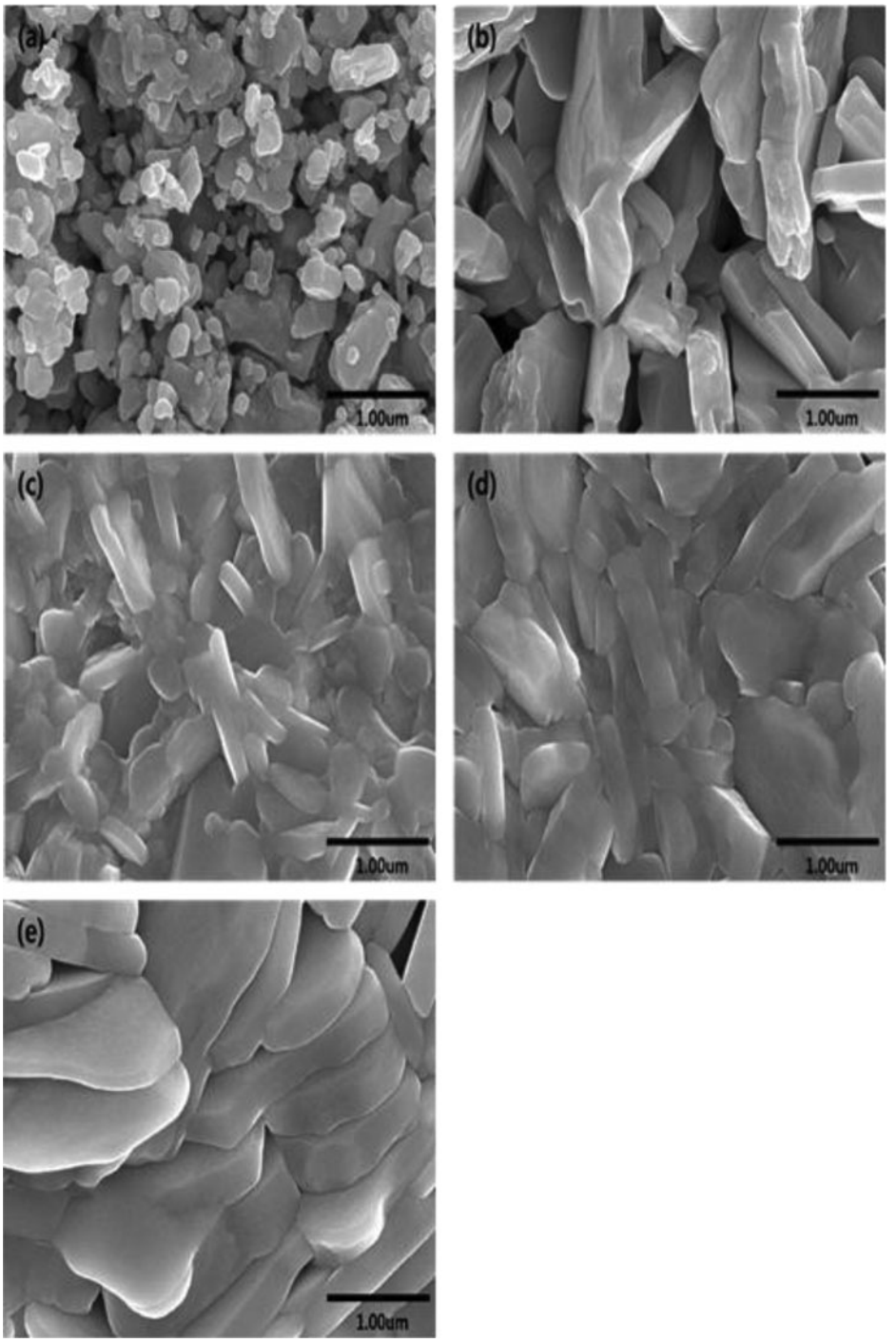


**Figure 2.** SEM images of Fe-BLT pellet sintered at (a) 700°C, (b) 800°C, (c) 900°C, (d) 1000°C, and (e) 1100°C

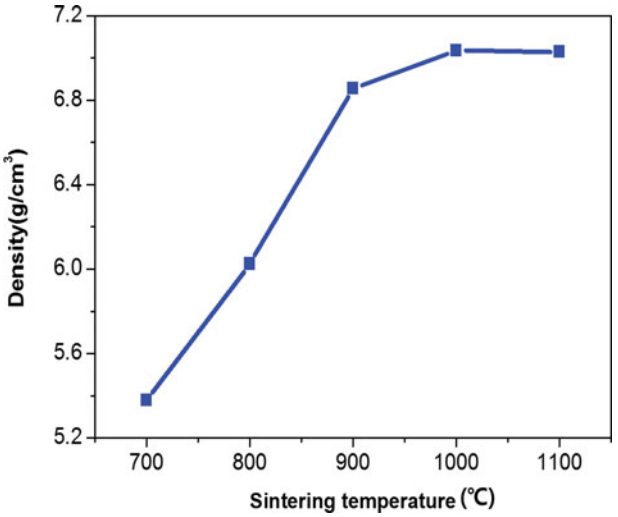


**Figure 3.** Density as a function of the sintering temperature.

sintered at various temperatures showed an increase in grain size and grain boundaries with increasing sintering temperature [20–22].

At 700°C, the microstructures consisted of plate-like grains and many porous. When sintered at 800°C, the size of the plate-like grains increased whereas many porous still remained. Hence, the sintering temperature was insufficient. When the sintering temperature was increased to 900°C, a relatively dense plate-like grain microstructure was observed without pores. On the other hand, apparent grain boundaries and junction were not observed in the microstructures. The sample sintered at 1000°C showed a similar structure to that sintered at 900°C, but the observed sample showed a very dense microstructure consisting of apparent grain boundaries and junction without pores. In addition, the plate-like grain size increased. When sintered at 1100°C, the isolated pore areas appeared.

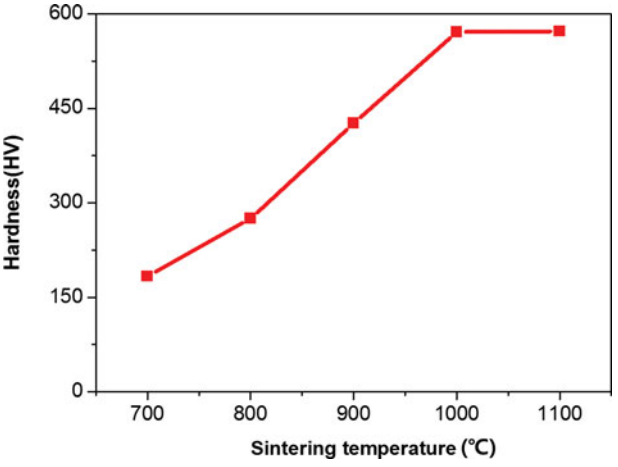


**Figure 4.** Vickers hardness as a function of the sintering temperature.

**Table 1.** 90°off–axis RF sputter process conditions

| Sputtering Condition | Value |
|---|---|
| RF Power | 50 W |
| Heating Temperature | Room temperature |
| Ar Partial Pressure | 135 mTorr |
| Input Ar:$O_2$ ratio | 3:1 |
| Deposition rate | 3 nm/min |



Figure 3 shows the density of the Fe-BLT pellets with different sintering temperature. This suggests that the sample sintered from 700 to 800°C exhibited low density, which can be explained by the pores at the grain boundaries with a plate-like shape. The density was increased with increasing temperature to 900 and 1000°C because of grain growth and the elimination of pores. On the other hand, the density of the sample sintered at 1100°C decreased slightly, possibly because the larger plate-like grains and structure with isolated pores caused greater difficulties in achieving a high packing density. These results suggest that Fe-BLT pellet could be well-sintered at 1000°C.

Figure 4 shows the Vickers hardness of the Fe-BLT pellet sintered at various temperature. The hardness increased from 700°C to 1000°C and it showed a constant value at 1000-1100°C, which was related directly to the density of the samples.

Using the Fe-BLT targets sintered at 1000°C, Fe-BLT films were deposited on glass substrates using 90°off–axis RF sputtering. Table 1 lists the value of the 90°off–axis RF sputtering conditions. The samples were sputtered from a 1-inch sized polycrystalline Fe-BLT target at RF power of 50W. The combined Ar and $O_2$ pressure was 135mTorr, and the substrate temperature and deposition time was room-temperature for 1 hour, respectively. The deposited film showed a mirror-like clean surface without particles on the surface. Using alpha step equipment (AS-500), the films were deposited a rate of 3 nm per minute. The Fe-BLT target sintered at 1000°C was found to be an appropriate target for thin film growth.

## Conclusion

This study examined the influence of the sintering temperature on the microstructural properties of Fe-BLT prepared under a normal air atmosphere. X-ray diffraction indicated that the crystallinity increased with increasing sintering temperature. On the other hand, the XRD patterns of the sample sintered at 1100°C showed an impurity phase and some other weak diffraction peaks. SEM images showed that the grain size and grain boundaries increased with increasing sintering temperature and no pores were observed. The density and Vickers hardness also increased with increasing sintering temperature due to grain growth and the elimination of pores. Therefore, the Fe-BLT pellet sintered at 1000°C was found to be the optimal sintering target for thin film growth.

## Acknowledgments

This study was supported by the Human Resources Development program (No. 20124030200010) of the Korea Institute of Energy Technology Evaluation and Planning

(KETEP) grant funded by the Korea government Ministry of Trade, Industry and Energy and Basic Science Research Program through the National Research Foundation of Korea (NRF) funded by the Ministry of Science, ICT & Future Planning (No. 2013005417).

## References

[1] Y. H. Xu and J. D. Mackenzie, (1992). *Integr. Ferroelectr. 1*, 17.
[2] R. Watton and P. Manning, (1998). *Proc. SPIE 3436*, 541.
[3] S. Sinharoy, H. Buhay, D.R. Lampe, M.H. Francombe, J. Vac, (1992). *Sci.Technol. A 10*, 1554.
[4] M. Yamaguchi, T. Nagamoto, (1997). *Thin Solid Films 300*, 299.
[5] P. H. Park, B. B. Kang, S. D. Bu, T. W. Noh, J. Lee and W. Jo, (1999). *Nature 401*, 682.
[6] W. S. Choi, M. F. Chisholm, D. J. Singh, T. Choi, G. E. Jellison, and H. N. Lee, (2012). *Nat.Comm. 3*, 689.
[7] M. Alexe, and D. Hesse, (2011). *Nat. Commun. 2*, 256.
[8] S. R. Basu, L. W. Martin, Y.-H. Chu, M. Gajek, R. Ramesh, R. C. Rai, X. Xu, and J. L. Musfeldt, (2008). *Appl. Phys. Lett. 92*, 091905.
[9] A. J. Hauser, J. Zhang, L. Mier, R. A. Ricciardo, P. M. Woodward, T. L.Gustafson, L. J. Brillson, and F. Y. Yang, (2008). *Appl. Phys. Lett. 92*, 222901.
[10] F. Gao, X. Chen, K. Yin, S. Dong, Z. Ren, F. Yuan, T. Yu, Z. Zou, J. M. Liu, (2007). *Adv.Mater.19*, 2889–2892.
[11] S. H. Hu, J. Chen, Z. G. Hu, G. S. Wang, X. J. Meng, J. H. Chu, N. Dai, (2004). *Mater. Res. Bull. 39*, 1223–1229.
[12] J. Y. Han, and C. W. Bark, to be published in Mol. *Cryst. Liq. Cryst.*
[13] C. W. Bark, (2013). *Met. Mater. Int. 19*, 1361–1364.
[14] S. D. Bu, B. S. Kang, B. H. Park and T. W. Noh, (2000). *Journal of the Korean Physical Society 36*, 9–12.
[15] P. Siriprapa, A. Watcharapasorn, and S. Jiansirisomboon, (2013). *Ceramics International 39*, 355–358.
[16] P. Siriprapa, A. Watcharapasorn, and S. Jiansirisomboon, (2009). *Journal of Microscopy Society of Thailand 23*, 99–102.
[17] P. C Sati, M. Arora, S. Chauhan, S. Chhoker and M. Kumar, (2014). *J. Phys. Chem. Solids. 75*, 105–108.
[18] D. C. Arnold, K. S. Knight, F. D. Morrison, and P. Lightfoot, (2009). *Phys. Rev. Lett. 102*, 027602.
[19] D. C. Arnold, K. S. Knight, G. Catalan, S. A. T. Redfern, J. F. Scott, P. Lightfoot, and F. D. Morrison, (2010). *Adv. Funct. Mater. 20*, 2116.
[20] S. Mahajan, O.P. Thakur, and C. Prakash, (2007). *Defence Science Journal 57*, 23–28.
[21] P. Jaiban, A. Rachakom, S. Jiansirisomboon, and A. Watcharapasorn, (2011). *Journal of the Microscopy Society of Thailand 4*, 20–23.
[22] P. Prayoonphokkharat, S. Jiansirisomboon, and A. Watcharapasorn, (2013). *Electronic Materials Letters 9*, 413–416.